Accurate Single-End Fault Location and Line-Length Estimation Using Traveling Waves

E. O. Schweitzer, III, A. Guzmán, M. Mynam, V. Skendzic, and B. Kasztenny
Schweitzer Engineering Laboratories, Inc.

C. Gallacher
Avista Utilities

S. Marx
Bonneville Power Administration

Presented at the
13th International Conference on Developments in Power System Protection
Edinburgh, United Kingdom
March 7–10, 2016

Accurate single-end fault location and line-length estimation using traveling waves

E. O. Schweitzer, III*, A. Guzmán*, M. Mynam*, V. Skendzic*, B. Kasztenny*, C. Gallacher†, S. Marx**

**Schweitzer Engineering Laboratories, Inc., 2350 NE Hopkins Court, Pullman, WA 99163 USA, armando@selinc.com*
†Avista Utilities, 1411 E Mission Ave., Spokane, WA 99202 USA,
***Bonneville Power Administration, 1350 Lindsay Boulevard, Idaho Falls, ID 83401 USA*

Keywords: fault locating, single-end method, traveling waves, reflections, time reference.

Abstract

Single-end fault locating using traveling waves can potentially be more accurate than double-end fault-locating methods. Traveling-wave reflections from taps or neighboring terminals can present a challenge to this approach, but characterizing these reflections ahead of time, using events such as line energization, simplifies the analysis. In addition to fault locating, traveling-wave recording can also be used for estimating line length. The analyses of field events, presented in this paper, show how we identified reflections for accurate fault location and line-length estimation. Line patrol staff have validated the results obtained using our methodology.

1 Introduction

Accurate fault locating is critical for the reliable operation of power systems. Identifying permanent faults is important for power system restoration; however, locating temporary faults with successful autoreclosing may not have a similar level of urgency. Traveling-wave-based fault location (TWFL) methods offer accuracy in the order of one to two tower spans, independent of the line length. This accuracy makes finding the damaged insulators comparatively less challenging and less time-consuming than using alternative methods such as impedance-based methods. When line patrols find and replace damaged insulators, reoccurrences of transient faults at the same locations are eliminated, which results in improved power system reliability.

The single-end TWFL method uses the time differences between the first arrived wave and the successive reflections from the fault and/or remote terminal to compute the fault location. This method is appealing because it depends only on local information. It does not require a communications channel and a precise, common time reference for the local and remote TW data. Although it may be more challenging to implement, the single-end TWFL method has less error than the double-end TWFL method because it estimates the first and reflected wave arrival times using only one hardware device and its internal clock. This provides a chance for some errors to self cancel. Furthermore, the single-end method is the only option available when energizing a faulted line. The challenge comes with identifying reflections, especially if wide-bandwidth voltage measurements are not available to isolate the incident TW from the measured voltage and current TWs.

This paper discusses a novel single-end TWFL method that uses current TWs to identify reflections from the fault, the remote end, and any discontinuity on the transmission line. The proposed algorithm excludes the reflections from neighboring stations, taps, and other discontinuities by using a reference train of TWs captured during one or more of these events: line energization, external faults, automatic reclosing (with and without faults), and external switching of reactor or capacitor banks. The algorithm uses this information along with the TW data captured during the fault to estimate the fault location. The TW event data also include information of the wave propagation time along the line. We use this information for determining the line length and distances between taps.

The proposed approach is applicable to overhead and tapped transmission lines. It is also suitable for underground and underground-overhead power line applications. We present data from a 181.61 km (112.85 mi), 115 kV tapped transmission line and a 117.11 km (72.77 mi), 161 kV two-end transmission line to demonstrate the validity of this method. These data, along with data captured during line energization and other reclosing events, provide enough information for accurate fault location and line-length estimation. We validate the TWFL estimation results with actual line patrol findings.

2 Reflected and transmitted TWs

When passing through a junction point (e.g., a tap on the line), incident current TWs are reflected and transmitted according to the characteristic impedances of the connected line segments, see Fig. 1. For the incident TW, i_1^I, the reflection Γ_i and transmission T_i coefficients are calculated by using (1) and (2) [1], [2].

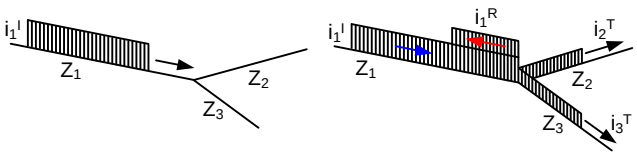

Fig. 1. Current TW passing through a junction point.

$$\Gamma_i = \frac{Z_1 - Z_P}{Z_1 + Z_P} \quad (1)$$

$$T_i = \frac{2 \cdot Z_1}{Z_1 + Z_P} \quad (2)$$

where Z_1 is the characteristic impedance of Segment 1, and Z_P is the equivalent impedance of the parallel of the characteristic impedances of Segments 2 and 3, Z_2 and Z_3, as shown in (3).

$$Z_P = \frac{Z_2 \cdot Z_3}{Z_2 + Z_3} \quad (3)$$

The reflected current, i_1^R, and transmitted currents, i_2^T and i_3^T, are calculated according to (4), (5), and (6), respectively.

$$i_1^R = \Gamma_i \cdot i_1^I \quad (4)$$

$$i_2^T = \frac{Z_P}{Z_2} T_i \cdot i_1^I \quad (5)$$

$$i_3^T = \frac{Z_P}{Z_3} T_i \cdot i_1^I \quad (6)$$

In Section 3, we discuss the challenges that the single-end TW fault-locating method faces because of transmission and reflection of TWs.

3 Single-end fault locating and line-length estimation

3.1 Fault location estimation

The single-end TW fault-locating method uses local TW arrival information from the first and the reflected waves [3], [4], and [5]. Fig. 2 shows that the TW reaching *L*, at t_{L1}, is both transmitted and reflected. The reflected wave reflects off the fault and travels back to *L*, arriving at time t_{L2}. The time $t_{L2} - t_{L1}$ is the travel time from *L* to the fault and back. Notice that the reflected wave from the remote terminal arrives at t_{L3}. To estimate fault location, this single-end fault-locating method uses the time difference between the first arrived TW and the successive reflection from the fault, as shown in (7).

$$m = \left(\frac{t_{L2} - t_{L1}}{2} \right) \cdot v \quad (7)$$

where:

t_{L1}, t_{L2} are the TW arrival times at *L*,
v is the TW propagation velocity.

We can, therefore, locate the fault using information from one end, as long as we are not confused by other reflected waves. For example, suppose that there is a short line right behind *L*, so short that its far end, *B*, is closer to *L* than the distance from *L* to the fault (see Fig. 3). In this case, the TW from *B* could reach *L* before t_{L2}. These TWs need to be sorted out depending on their direction in order to accurately locate the fault.

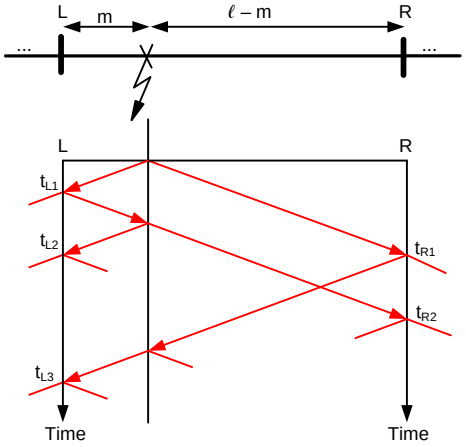

Fig. 2. Lattice diagram showing incident, reflected, and transmitted TWs and arrival times at the local terminal to estimate line length and fault location. ℓ is the line length and m is the distance to the fault from *L*.

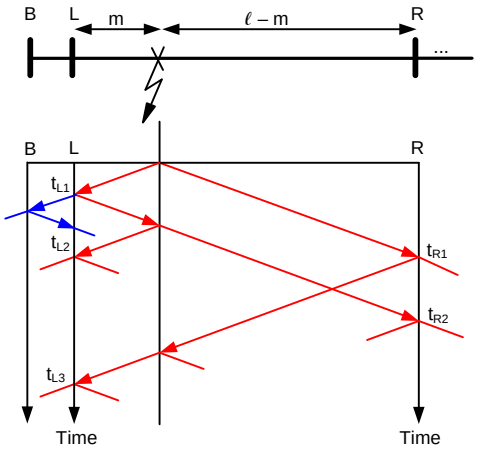

Fig. 3. Reflection from the external network element (*B*) reaches *L* before reflection from the fault.

These extra TW reflections are network dependent. Schweitzer successfully developed a single-end fault locator for high-voltage dc (HVDC) lines [3], [4]. The device uses voltage and current to separate incident and reflected TWs.

Using only currents for TW fault-locating limits our ability to separate the incident and reflected TWs. Under these limitations, we use an alternative approach in which we discard reflections from known junction points and identify reflections from the fault for simplifying the single-end fault-locating analysis. For identifying reflections from known terminations (network topology), we use TW data captured during the following power system events:

- Line energization
- External faults
- Automatic reclosing
- External reactor/capacitor switching
- Previous line faults

The field cases in Sections 5 and 6 show oscillograms with current TWs recorded from line energization and faults.

3.2 Line-length estimation

In addition to fault-locating information, single-end TW event reports include information required for estimating the line length. This estimated length provides feedback to the line patrol staff for verifying the actual line length used for finding faults along the line. Fig. 2 illustrates TW arrival times at the local terminal L from the fault (t_{L1} and t_{L2}) and from the remote terminal R (t_{L3}). The time $t_{L3}-t_{L1}$ is two times the travel time along the line minus two times the time from the fault to L. The time $t_{L3}-t_{L1}$ corresponds to the distance 2ℓ–2m. With these TW arrival times, we use (8) to estimate the line length.

$$\ell = \frac{v}{2}\left[\left(t_{L2}-t_{L1}\right)+\left(t_{L3}-t_{L1}\right)\right] \tag{8}$$

If we divide (7) by (8), we can express the per unit length fault location in terms of the $t_{L2}-t_{L1}$ and $t_{L3}-t_{L1}$ delays, as shown in (9).

$$\frac{m}{\ell} = \frac{(t_{L2}-t_{L1})}{(t_{L2}-t_{L1})+(t_{L3}-t_{L1})} \tag{9}$$

4 Determining TW arrival times using a differentiator smoother [6]

This approach originated in “leading-edge tracking” techniques used in radar [7]. It overcomes most effects of signal distortion and allows for interpolation between samples. This approach was first used in fault locating in the dc fault locator described in [3] and [4]. Subsequent implementation of the differentiator smoother in the ac fault locator described in [6] further proved this approach in the field.

Fig. 4a shows a block diagram suitable for demonstrating the method. The current is first low-pass filtered or smoothed; then its output is differentiated. Smoothing reduces the effects of waveform distortions and causes the current rising edge to smooth out and become less steep. “Softening” the rising edge at first may seem contrary to the objective of determining the time of arrival; however, it spreads the edge over several samples, making the time-interpolation process possible.

The smoothed waveform is then differentiated, turning the step-like current waveform into a soft pulse-like shape. That pulse-like derivative has its peak at the instant of the steepest slope of the current waveform. The peak of the derivative is relatively insensitive to amplitude changes, being about halfway along the edge, no matter how “tall” the current step is. Fig. 4c shows the derivative output in detail and adds the points in time where the samples were taken. It also shows a pair of lines; their intersection is an excellent measure of t_A, the TW arrival time.

When using filters to smooth the derivative of the current, the output resembles a parabola, as shown in Fig. 4b and Fig. 4c. Therefore, in our implementation, we use a parabola-based interpolation method for calculating the arrival time. The algorithm selects a few samples prior to the peak sample and a few samples following the peak. It further uses the least-squares estimation (LSE) method to fit a parabola to the selected points, including the maximum sample, and calculates the arrival time (t_A) using the best-fitting parabola (see Fig. 5).

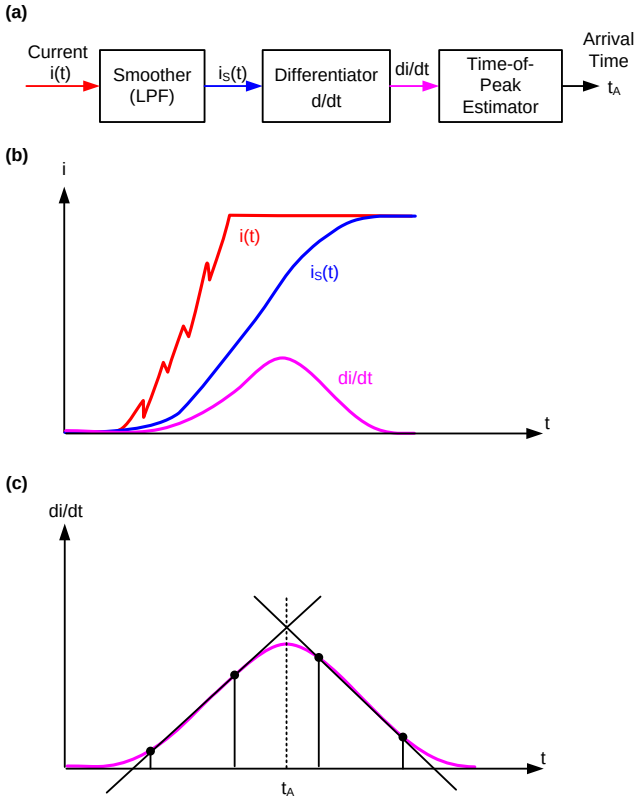

Fig. 4. Differentiator smoother: (a) block diagram, (b) typical waveforms, and (c) time-of-peak estimation.

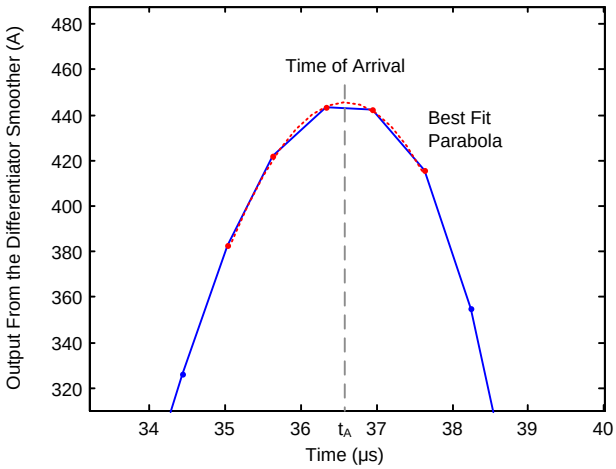

Fig. 5. Accurate time-stamping of the TW using the best-fit parabola.

5 Single-end TW fault locating using field events from a line with taps

5.1 Brasada-Harney Line

Fig. 6 shows the 115 kV, 181.61 km (112.85 mi) Brasada-Harney transmission line along with its neighboring system.

The tap locations are terminated with transformers serving distribution feeders. The line is a section of a longer transmission path (about 422 km or 262 mi), with several tapped loads, in Central and Eastern Oregon. Half of the path is 115 kV and the rest of the path is 138 kV. The terrain consists of rural high-altitude desert and irrigated farm land. Historically, the line experiences ten or more faults per year. In many cases, faults on the line have been attributed to insulator flashover caused by lightning, contamination from wildlife, or dust accumulation mixed with rain or dew. The relays successfully reclosed for all these faults.

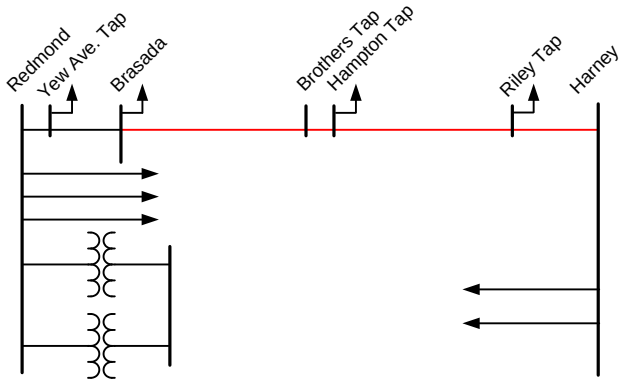

Fig. 6. 115 kV transmission network includes the Brasada-Harney line with adjacent lines and taps.

5.1.1 Using TWs captured during line energization for identifying TW reflection from a fault

To address the challenge of identifying and excluding the reflections from the neighboring stations, tap locations, and other discontinuities, we used a reference train of waves captured during line energization with the remote terminal open. We also could have captured the reference train of waves during external faults or automatic reclosing (without a fault). The reference waves provide information on the line topology and adjacent taps. By using these reference waves along with the waves captured during an internal fault, and aligning the first wave captured from both events, we were able to discard the common reflections from both events. Following this approach, we identified the reflection from the fault. The reflections could be directly from the fault or from the wave reflected from the remote terminal.

Fig. 7 shows the phase current TWs captured during line energization that we used as the reference signal. Note that the closure of the B-phase and C-phase poles provided a train of waves showing the location of taps and other terminations. In this line energization event, the A-phase pole closed at the zero voltage point on the wave. Fig. 8 shows the train of current TWs recorded at Brasada during a line energization aligned with the A-phase current TWs recorded during an A-phase-to-ground fault.

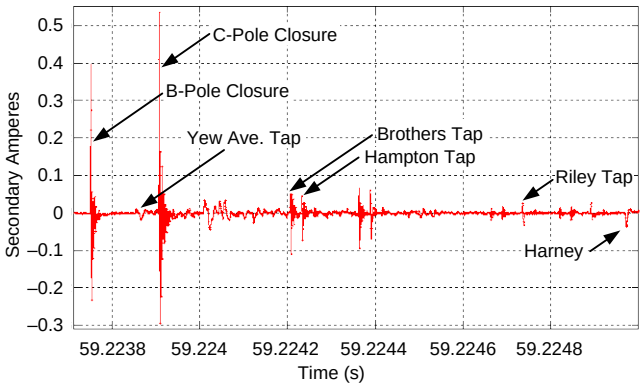

Fig. 7. Line energization event identifying TW reflections from taps resulting from the B-phase pole closure.

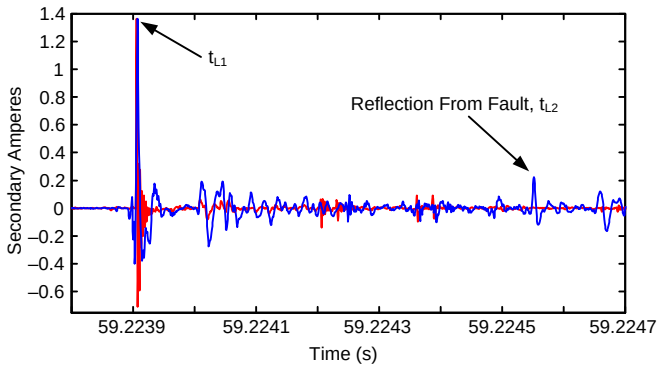

Fig. 8. A-phase current TWs for an A-phase-to-ground fault aligned with the current TWs recorded during line energization.

Once we identified the reflection from the fault using the above concept, we used the wave arrival times associated with the first arrived wave (t_{L1} = 59.223906323 s) and the reflected wave (t_{L2} = 59.224552026 s) from the fault to compute the fault location using (7). With v = 0.99225 times the speed of light, we estimated the fault location at 96.04 km (59.68 mi). Additionally, since we knew the location of the line terminations and taps, we provided the line patrol staff with the fault location from the Hampton tap.

5.1.2 Using impedance-based fault locating for identifying TW reflection from a fault

We used the event reports from a C-phase-to-ground fault close to the Brasada terminal for analyzing operating frequency signals and TWs. For this event, the fault contribution from Harney was so low that the line relay at Harney operated after the Brasada breaker opened (sequential tripping occurred). Fig. 9 shows the recorded phase currents and voltages and Fig. 10 shows the TW currents recorded at the Brasada terminal.

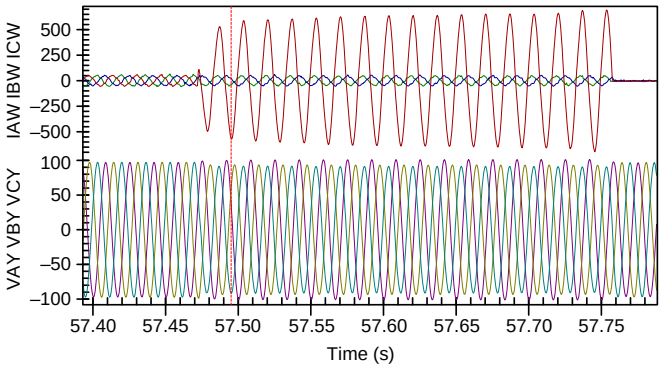

Fig. 9. Currents (primary A) and voltages (primary kV) for a C-phase-to-ground fault for performing the first fault location estimation.

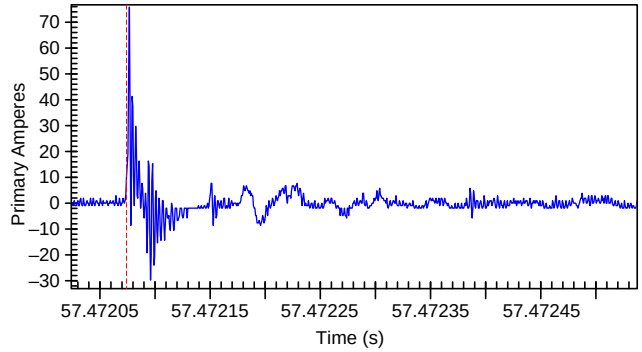

Fig. 10. Current TWs for a C-phase-to-ground fault used for fault locating.

For this event, we used a single-end impedance-based method [8] to identify the reflection from the fault. As mentioned earlier, this event resulted in sequential tripping, which translates to having the Harney terminal feeding the fault with the Brasada terminal open (radial system). This system condition is well suited for the single-end impedance-based method. We used the phase voltages and currents captured at the Harney terminal in the radial system condition along with the positive- and zero-sequence line impedances, and computed the fault location at 170.43 km (105.90 mi) from Harney and 11.18 km (6.95 mi) from Brasada. With this impedance-based single-end fault-location estimate, we predicted the reflection associated with the fault to be at about t = 57.472114909 s. We found the reflection at t_{L2} = 57.472152205 s. Fig. 11 shows the first wave and the reflections from the fault and from the Yew Avenue tap (located right behind the Brasada terminal).

After identifying the reflection from the fault, we calculated the fault location by using the arrival time of the first TW and the time associated with the first reflection from the fault: t_{L1} = 57.472077325 s and t_{L2} = 57.472152205 s. The estimated fault location was 11.13 km (6.92 mi) from Brasada. This fault location translates to tower 8/6 (eighth tower after the sixth mile), where line patrol staff found the flashed over insulator shown in Fig. 12.

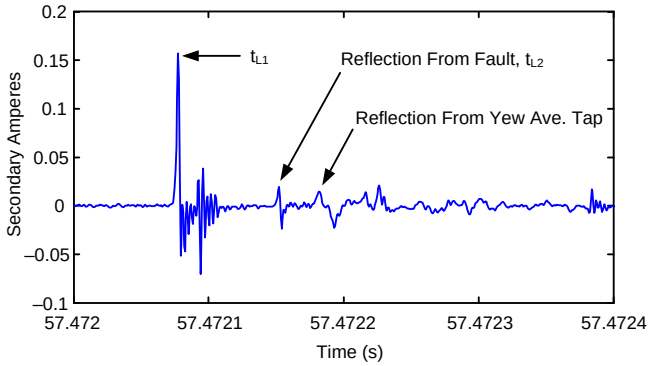

Fig. 11. C-phase alpha current during the C-phase-to-ground fault recorded at the Brasada terminal along with the identified reflections from the fault.

Fig. 12. Flashed-over insulator on the C-phase, tower 8/6 (eighth tower after the sixth mile) of the Brasada-Harney line.

6 Line-length estimation using a field event

We analyzed a field event of a B-phase-to-ground fault on the 161 kV, 117.112 km (72.77 mi) Goshen-Drummond line (see Fig. 13) where we knew the fault location for estimating the line length; the fault occurred because of gunshots to insulators. The line patrol reported the fault location at 61.41 km (38.16 mi) from Goshen and 55.70 km (34.61 mi) from Drummond.

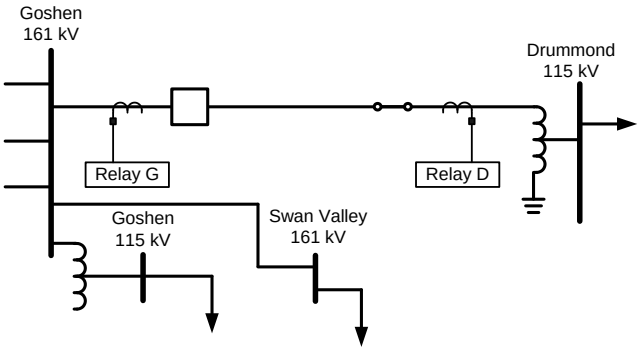

Fig. 13. Transmission network includes the Goshen-Drummond line and CT and relay connections. Notice that the line termination at Drummond is an autotransformer [9].

Fig. 14 shows the lattice diagram for this fault and corresponding alpha-mode B-phase TW currents as seen by the Goshen and Drummond relays. We used the algorithm to estimate the wave arrival times described in Section 4. The diagram shows the filtered currents according to this algorithm. In these plots, you can clearly see the local and remote reflections at Goshen: the first reflected peak comes from Drummond and the second reflected peak comes from the fault. Using the following data from Goshen, we estimated a line length of 117.44 km (72.97 mi) by using (8) and a fault location of 61.22 km (38.04 mi) from Goshen by using (7).

t_{L1} = 36.832684635 s

t_{L2} = 36.833097963 s

t_{L3} = 36.833064209 s

v = 0.98811 times the speed of light

The estimated line-length error is 0.28 percent or 328 m; this error could be attributed to conductor sagging.

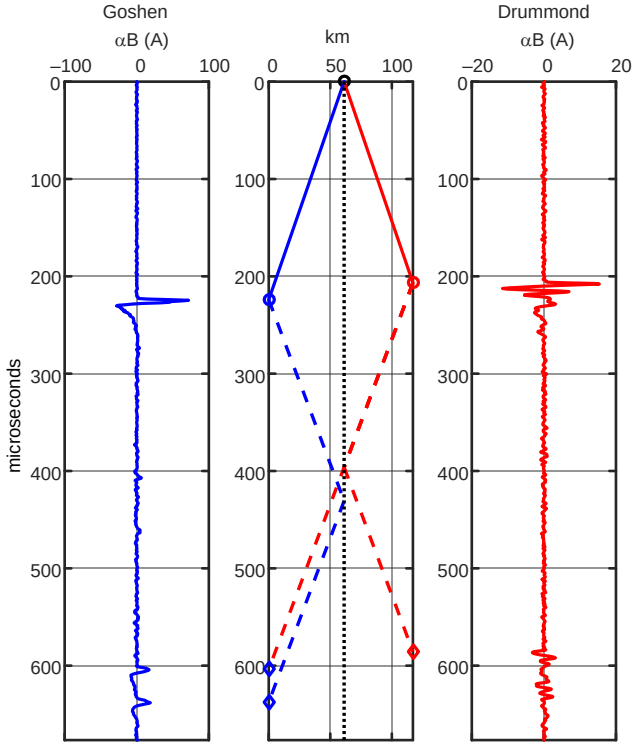

Fig. 14. TWs for a B-phase-to-ground fault on the Goshen-Drummond line used for estimating line length.

7 Conclusion

The analyses of the field events presented in this paper demonstrate that the fault locating algorithm that uses the differentiator-smoother and wave arrival time estimator, together with the presented method for identifying reflections from the fault, simplify fault-locating analysis and provide accurate single-end TW fault location estimations (errors of less than 200 m). Line patrol findings validated these results.

Field event analysis also demonstrates that TW event reports provide information for estimating line length within 0.3 percent. Conductor sagging is the main contributor of the difference between the geographical and actual line lengths.

References

[1] L. V. Bewley, *Traveling Waves on Transmission Systems*. Dover Publications, Mineola, NY, 1963.

[2] A. Greenwood, "Electrical Transients in Power Systems," 2nd Edition, John Wiley & Sons, Inc., ISBN 0-471-62058-0, 1991.

[3] M. Ando, E. O. Schweitzer, III, and R. A. Baker, "Development and Field-Data Evaluation of Single-End Fault Locator for Two-Terminal HVDC Transmission Lines, Part I: Data Collection System and Field Data," *IEEE Transactions on Power Apparatus and Systems*, Vol. PAS–104, Issue 12, December 1985, pp. 3524–3530.

[4] M. Ando, E. O. Schweitzer, III, and R. A. Baker, "Development and Field-Data Evaluation of Single-End Fault Locator for Two-Terminal HVDC Transmission Lines, Part II: Algorithm and Evaluation," *IEEE Transactions on Power Apparatus and Systems*, Vol. PAS–104, Issue 12, December 1985, pp. 3531–3537.

[5] M. Aurangzeb, P. A. Crossley, and P. Gale, "Fault Location on a Transmission Line Using High Frequency Travelling Waves Measured at a Single Line End," proceedings of the 2000 IEEE Power Engineering Society Winter Meeting, Vol. 4, Singapore, January 2000, pp. 2437–2442.

[6] E. O. Schweitzer, III, A. Guzmán, M. V. Mynam, V. Skendzic, B. Kasztenny, and S. Marx, "Locating Faults by the Traveling Waves They Launch," proceedings of the 40th Annual Western Protective Relay Conference, Spokane, WA, October 2013.

[7] F. E. Nathanson, *Radar Design Principles: Signal Processing and the Environment*, McGraw-Hill Book Co., 1969.

[8] E. O. Schweitzer, III, "A Review of Impedance-Based Fault Locating Experience," proceedings of the 15th Annual Western Protective Relay Conference, Spokane, WA, October 1988.

[9] S. Marx, B. K. Johnson, A. Guzmán, V. Skendzic, and M. V. Mynam, "Traveling Wave Fault Location in Protective Relays: Design, Testing, and Results," proceedings of the 16th Annual Georgia Tech Fault and Disturbance Analysis Conference, Atlanta, GA, May 2013.